ChemComm

Accepted Manuscript

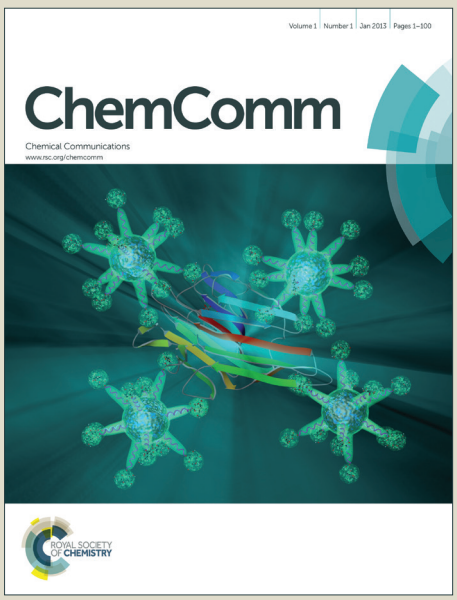

ROYAL SOCIETY OF CHEMISTRY

www.rsc.org/chemcomm

Journal Name

COMMUNICATION

Se-doped MoS_2 nanosheet for improved hydrogen evolution reaction

Received 00th January 20xx,
Accepted 00th January 20xx

DOI: 10.1039/x0xx00000x

www.rsc.org/

Xianpei Ren,[a] Qiang Ma,[a] Haibo Fan,[a, c] Liuqing Pang,[a] Yunxia Zhang,[a] Yao Yao,[a] Xiaodong Ren,[a] Shengzhong (Frank) Liu[a, b,*]

Thanks to the increase in number of active sites and enhanced conductivity, the Se-doped MoS_2 has excellent catalytic activity with a lower overpotential of 140 mV and a smaller Tafel slope of 55 mV/dec, exhibiting enhanced catalytic performance compared with that of pristine MoS_2. This work offers an attractive strategy to improve HER activity of MoS_2-based catalysts.

With very high energy density, hydrogen is considered as an ideal clean energy carrier that generates only water after its combustion.[1] The environmentally friendly electrocatalytic water-splitting is an important process for the hydrogen production. Conventionally, Pt-group metals are the most efficient electrocatalysts for the hydrogen evolution reaction (HER), but their limited resource and extremely high cost hinder their commercial application of this technology.[2, 3] Thus, it is desirable, no matter how challenging it is, to find inexpensive alternatives with high electrocatalytic activity to replace the Pt in the HER catalysts. Recently, nanostructured molybdenum sulfides (MoS_2) have been identified as potential substitutes for the Pt-group catalysts because the free energy of atomic hydrogen bonding to the sulfur edge of the MoS_2 structure is very close to that of Pt.[4-6] However, the catalytic HER performance of MoS_2 is currently limited by availability of number of the active sites and poor conductivity.[7-9]

There have been enormous attempts focusing on the improvement of either the number of active sites or the conductivity of MoS_2 electrocatalysts to enhance their HER activity. For the former one, increasing the active edge area of the MoS_2 by introducing nanoscale is an efficient strategy, for example, ultrathin MoS_2 nanoplates,[10] defect-rich MoS_2 nanosheets,[11] and MoS_2 quantum dots,[12] are used to obtain good catalytic performance. For the second one, the catalysts were loaded on highly conductive matrices, such as carbon nanotubes,[13] conductive polymer and graphene,[14-18] to form MoS_2-based hybrids or composites, and exhibit much higher catalytic activity than their pure MoS_2 counterparts. Meanwhile, the metallic 1T-MoS_2 shows better HER performance than the semiconducting 2H-MoS_2 phase.[19] However, the 1T-MoS_2 is thermodynamically metastable and turns into 2H-MoS_2 upon heating at moderate temperatures or aging in air.[20]

It is also found that the HER activity of MoS_2 electrocatalysts can be tuned through tailoring their chemical composition. For example, cobalt or nickel doping, and vanadium doping all can promote the electrocatalytic performance of MoS_2.[21, 22] Inspired by the inventions, we believe that the anion-doping to MoS_2 may also be used to improve the HER activity, such as selenium (Se) doping. At least the Se atom doped into the frameworks of MoS_2 will improve the electrical conductivity because of more metallic nature of Se. This factor motivated our curiosity in exploring the use of Se-doped MoS_2 materials as catalysts for HER.

Herein we described our success in preparation of Se-doped MoS_2 nanosheets via a facile annealing process using diphenyl diselenide (DDS) as the Se dopant. The overall formation process is depicted in Fig. 1a. More details on the synthesis procedure is given in the experimental section (see the ESI†). Benefiting from the high active edge sites and electronic conductivity by Se doping, the Se-doped MoS_2 exhibits an excellent electrocatalytic activity for the HER with substantial current densities and a small Tafel slope of 55 mV/dec.

Fig. 1b shows the XRD patterns of pristine MoS_2 and Se-doped MoS_2 nanosheets. All peaks can be assigned to hexagonal 2H-molybdenum dichalcogenide with no discernible impurities, revealing the high purity of the product. After Se doping, all main diffraction peaks slightly shifted toward smaller diffraction angles (see Fig. 1c, Fig. S1a-c), indicating that there is an increase in the interplanar distance as the Se atom is larger than S. Besides, it is also clear that the XRD

[a] Key Laboratory of Applied Surface and Colloid Chemistry, National Ministry of Education; Institute for Advanced Energy Materials, School of Materials Science and Engineering, Shaanxi Normal University, Xi'an 710119, China. E-mail: szliu@dicp.ac.cn
[b] Dalian Institute of Chemical Physics, Dalian National Laboratory for Clean Energy, Chinese Academy of Sciences, Dalian, 116023, China
[c] School of Physics, Northwest University, Xi'an 710069, China
Electronic Supplementary Information (ESI) available: [details of any supplementary information available should be included here]. See DOI: 10.1039/x0xx00000x

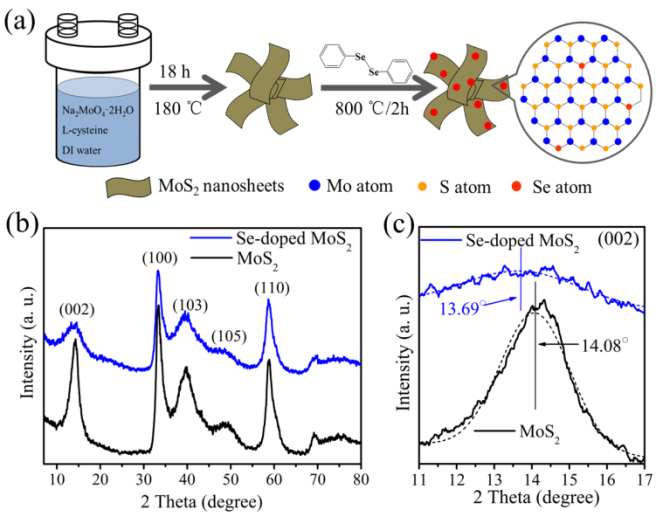

Fig. 1 (a) Schematic illustration of synthesis procedure for the Se-doped MoS_2 nanosheets. (b) XRD and (c) the enlarged (002) crystal plane of MoS_2 and Se-doped MoS_2 nanosheets; For (c), the solid lines are experimental data and the dotted lines are the corresponding Gaussian fittings.

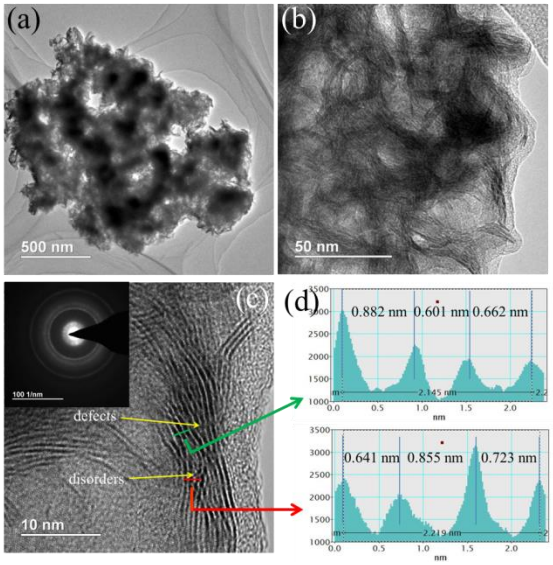

Fig. 2 (a and b) TEM images of Se-doped MoS_2 nanosheets. (c) High-magnification TEM image and (inset) the corresponding SAED patterns of Se-doped MoS_2 nanosheets. (d) The lattice distances of the labeled green and red lines in (c), HRTEM shows the spacing between adjacent (002) planes.

peaks of the Se-doped MoS_2 are broader and weaker in intensity (Fig. 1b and c), indicating that reducing the average grain size and the crystallinity, and increasing defective and disorderly structures in the Se-doped MoS_2 due to their open edges after Se doping.

The morphology and detailed microstructure of the Se-doped MoS_2 was studied by transmission electron microscopy (TEM) and high-resolution TEM (HRTEM) images and compared to those of pristine MoS_2 (Fig. 2 and Fig. S2). It shows that the basic morphology of nanosheets was retained after the Se doping. Fig. 2b reveals the lamellar structure and a large number of exposed edge sites of the (002) plane of Se-doped MoS_2. Comparing the HRTEM images of pristine and Se-doped MoS_2 (Fig. 2c and Fig. S2b), it appears that: (1) Se-doped MoS_2 shows a more disorderly and defective lattice fringes, indicating the disordering of atomic arrangements and the reduced crystallinity, as confirmed by the corresponding electron diffraction pattern (inset of Fig. 2c); (2) Se-doped MoS_2 shows slightly different spacing between adjacent (002) planes. As shown in Fig. 2d, the red line covers 2.145 nm in length and scan spans 3 different spacing of 0.882 nm, 0.601 nm and 0.662 nm, respectively; the green line covers 2.219 nm in length and scan spans 3 different spacing of 0.641 nm, 0.855 nm and 0.723 nm, respectively. It is apparent that the Se doping has caused lattice spacing expanded from 0.60 nm to over 0.88 nm, as witnessed by the XRD results. It should be noted that this disordered and defective lattice structure is desired for us for it generates increased number of active edge sites and improved overall catalytic activity for HER.

Fig. S3 shows Raman spectra of Se-doped MoS_2 using 532 nm laser excitation. Two characteristic peaks, in-plane (E^1_{2g}) and vertical plane (A_{1g}), are clearly resolved at ~378 cm^{-1} and 403 cm^{-1}.[23] By introducing Se, both peaks are shifted to lower frequency and intensity reduced. The frequency shift is caused by the interaction between S and Se atoms, leading to softened Mo-S vibration and decreased frequency;[24, 25] Meanwhile, the reduced Raman intensity is likely a consequence of the change in lattice symmetry that determines the matrix elements and selection rules for Raman active vibrational modes.[26] In addition, Se-doped MoS_2 gives a larger E^1_{2g}/A_{1g} value than that of pristine MoS_2 (0.56 vs. 0.46), resulting in abundant edge structures.[27, 28]

X-ray photoelectron spectroscopy (XPS) was used to examine the chemical states and the Se content in the as-synthesized Se-doped MoS_2 nanosheets. Fig. 3a-c illustrates the Mo 3d, S 2p, and Se 3d high resolution spectra of Se-doped MoS_2. As shown in Fig. 3a, two characteristic peaks located at 229.3 eV and 232.5 eV are attributed to Mo^{4+} $3d_{5/2}$ and $3d_{3/2}$, suggesting the dominance of Mo^{4+} in the sample.[29] The peak at 162.2 and 163.4 eV in Fig. 3b are attributed to S^{2-} $2p_{3/2}$ and S^{2-} $2p_{1/2}$, respectively.[30] The peak at 161.0 eV is attributed to Se $3p_{3/2}$. The Se 3d peak is split into well-defined $3d_{5/2}$ and $3d_{3/2}$ peaks at 54.5 and 55.4 eV (Fig. 3d),[31] a well known characteristic of substitutional doping of Se to S, in comparison of S occupying the interstitial sites of MoS_2. Quantification analysis of the Se 3d and S 2p peaks gives the Se doping concentration in MoS_2 ∽5.7%. Moreover, typical scanning transmission electron microscopy (STEM) and elemental mapping images of Se-doped MoS_2 nanosheets are presented in Fig. 3d-g, it is clear that all elements (Mo, S, Se) are distributed uniformly in the sample. It is worth noting that even high resolution ADF analysis did conclude not-so-uniform Se distribution in an earlier report by Y. Gong, [32] for probing size ~ 500 nm using low resolution TEM mapping for present

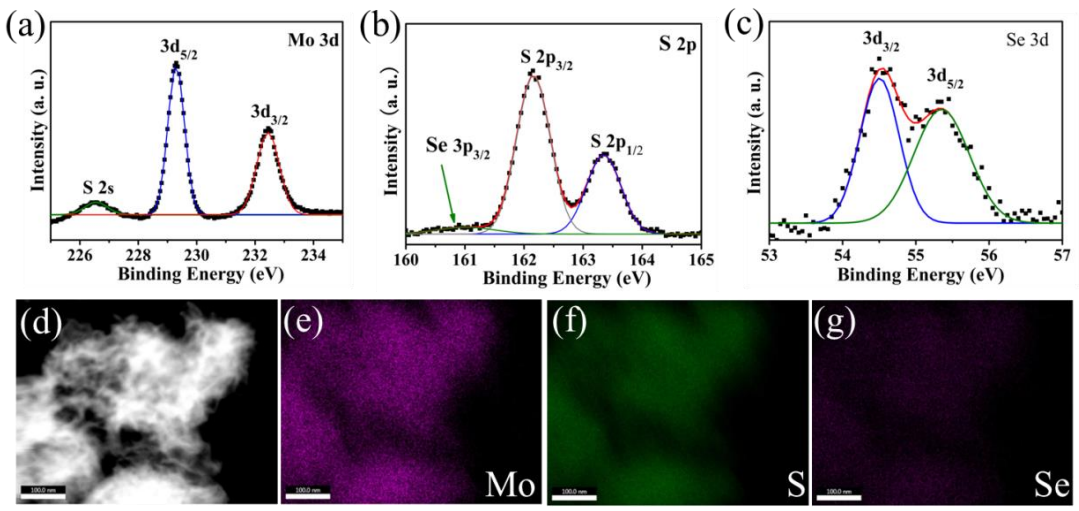

Fig. 3 High-resolution XPS spectra of Mo 3d (a), S 2p and Se 3p (b), Se 3d (c) of the Se-doped MoS_2 nanosheets. (d) STEM-bright field image of the Se-doped MoS_2 nanosheets. (e-g) Elemental mapping of Mo, S and Se from the region shown in (d), respectively (scale bars, 100 nm).

samples, all three elements (Mo, S, Se) show fairly consistent distribution.

The HER using MoS_2 and Se-doped MoS_2 nanosheet catalysts were measured using the standard three-electrode electrochemical configuration in 0.5 M H_2SO_4. The catalysts were loaded on glassy carbon carrier and the electrolyte de-aerated with N_2, and more details are described in the Experimental section. For comparison, commercial Pt electrode was used as the reference. As shown in Fig. 4 a, the Pt catalyst exhibits extremely high HER catalytic activity with a very low onset overpotential ($\eta \approx$-40 mV). Pristine MoS_2 displays weak HER performance with a high onset potential and a weak cathodic current density. In contrast, the Se-doped MoS_2 shows much higher HER activity with a small onset overpotential ~-140 mV, beyond this potential the cathodic current increased rapidly. It is clear that at η= -400 mV, the Se-doped MoS_2 exhibits an extremely large cathodic current density 42.7 mA/cm^2, ~4 times larger than what observed in MoS_2 (11.2 mA/cm^2).

To further study the catalytic activity of Se-doped MoS_2 nanosheets, Tafel plots derived from the polarization curves were used to determine the Tafel slopes. As shown in Fig. 4 b, the Tafel slope of the Pt catalyst is ~35 mV/dec, very similar to what reported in literature.[33] The Tafel slope of Se-doped MoS_2 is 55 mV/dec, even though it is indeed larger comparing to Pt, it is much smaller than that of the pristine MoS_2 (89 mV/dec). Considering that not only the onset overpotential is reduced, its Tafel slope is much improved, the Se-doped MoS_2 is clearly demonstrated with much enhanced catalytic activity.

Notably, the HER performance of the obtained Se-doped MoS_2, within the context of onset potential (-140 mV), and Tafel slope (55 mV/dec), is markedly better than those of un-doped MoS_2 catalysts, such as MoS_2 nanosheets (-180 mV, 87 mV/dec), nanosized bulk MoS_2 (-280 mV, 82 mV/dec), MoS_2 nanoparticles (-160 mV, 77 mV/dec), and comparable to other doped MoS_2 catalysts, such as V-doped MoS_2 (-13[illegible] mV, 60 mV/dec) and oxygen-incorporated MoS_2 (-120 mV, 55 mV/dec). However, there are indeed reports using composite[illegible] to achieve even better activity (Table S1).

The enhanced catalytic activity of Se-doped MoS_2 may be attributed to two factors: (1) Incorporation of Se into Mo[illegible]$_2$ reduces the average grain size, therefore resulting in mor[illegible] active edge sites, as confirmed by the TEM, XRD and Rama[illegible] measurements. (2) The Se atoms doped into MoS_2 improve th[illegible] electrical conductivity as Se is more metallic than S. Thi[illegible] hypothesis was further confirmed by electrochemica[illegible] impedance spectroscopy (EIS) measurements in 0.5 M H_2SO_4 (Fig. 4c). The Se-doped MoS_2 only showed a charge transfe[illegible] resistance (Rct) 650 Ω, much smaller than that of MoS_2 (1945 Ω), demonstrating that Se doping dramatically enhances [illegible] electron transfer.

The effects of Se dopant concentration on the HER performance of Se-doped MoS_2 were then probed by LS[illegible] measurements. Fig S4 shows that the HER performance of th[illegible] Se-doped MoS_2 increased with the Se content. Other than th[illegible] HER activity, stability is another important characteristic use[illegible] to evaluate an electrocatalyst. To investigate the stability o[illegible] the Se-doped MoS_2, we determined the HER activity of the Se-doped MoS_2 at a constant potential of -0.25 V for 9000s. After a long period of 9 000s, only a slight decrease in the curren[illegible] density was observed for the Se-doped MoS_2, suggesting superior stability (Fig. 4d).

In conclusion, we have developed an effective hig[illegible] temperature annealing method for the synthesis of Se-doped MoS_2 nanosheets. The Se-doped MoS_2 exhibits promising HE[illegible] activity with a low overpotential of approximately 140 mV, [illegible] large cathodic current density, and a small Tafel slope of 55 mV/dec, much better than the undoped MoS_2 catalyst. W[illegible] attribute the improved performance to thenhanced electrical conductivity that facilitates rapid electron transfer from the

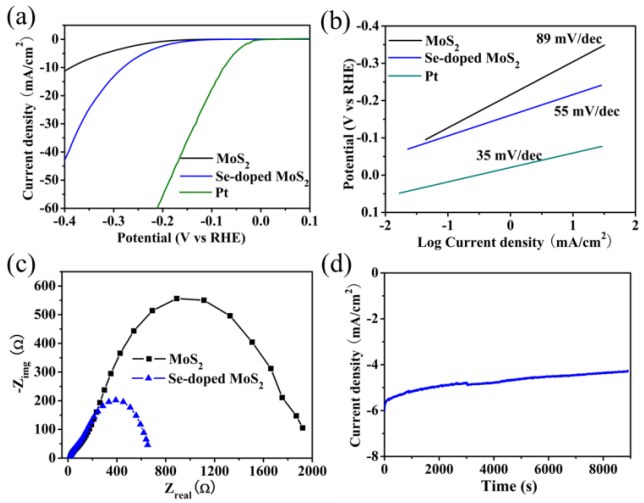

Fig. 4 HER performance of MoS_2 and Se-doped MoS_2 nanosheet catalysts. (a) Polarization curves, (b) Tafel plots of MoS_2, Se-doped MoS_2 and Pt electrode at scan rate 10 mV/s in 0.5 M H_2SO_4. (c) EIS Nyquist plots of MoS_2 and Se-doped MoS_2. (d) The durability test of Se-doped MoS_2 with applied voltage of -250 mV vs. RHE over 9, 000s in 0.5 M H_2SO_4.

electrode to the catalyst and the improved active edge sites.

The authors acknowledge support from the National University Research Fund (GK261001009), the Changjiang Scholar and Innovative Research Team (IRT_14R33), the Overseas Talent Recruitment Project (B14041) and the Chinese National 1000-talent-plan program.

Notes and references

1 A. Paracchino, V. Laporte, K. Sivula, M. Grätzel, E. Thimsen, Nat. Mater., 2011, **10**, 456-461.

2 Y. Hara, N. Minami, H. Matsumoto, H. Itagaki, Appl. Catal. A-Gen., 2007, **332**, 289-296.

3 B. Fang, J. H. Kim, J. S. Yu, Electrochem. Commun., 2008, **10**, 659-662.

4 H. I. Karunadasa, E. Montalvo, Y. Sun, M. Majda, J. R. Long and C. J. Chang, Science, 2012, **335**, 698-702.

5 A. B. Laursen, S. Kegns, S. Dahl and I. Chorkendorff, Energy Environ. Sci., 2012, **5**, 5577-5591.

6 T. Wang, L. Liu, Z. Zhu, P. Papakonstantinou, J. Hu, H. Liu and M. Li, Energy Environ. Sci., 2013, **6**, 625-633.

7 J. Kibsgaard, Z. Chen, B. N. Reinecke, T. F. Jaramillo, Nat. Mater., 2012, **11**, 963-969.

8 T. F. Jaramillo, K. P. Jørgensen, J. Bonde, J. H. Nielsen, S. Horch, Science, 2007, **317**, 100-102.

9 X. Guo, G. Cao, F. Ding, X. Li, S. Zhen, Y. Xue, Y. Yan, T. Liu and K. Sun, J. Mater. Chem. A, 2015, **3**, 5041-5046.

10 Y. Yan, B. Xia, X. Ge, Z. Liu, J. Y. Wang and X. Wang, ACS Appl. Mater. Inter., 2013, **5**, 12794-12798.

11 J. Xie, H. Zhang, S. Li, R. Wang, X. Sun, Mi. Zhou, J. Zhou, X. W. Lou, Y. Xie, Adv. Mater., 2013, **25**, 5807-5813.

12 X. Ren, L. Pang, Y. Zhang, X. Ren, H. Fan and S. F. Liu, J. Mater. Chem. A, 2015, **3**, 10693-10697.

13 Y. Shi, Y. Wang, J. I. Wong, A. Y. S. Tan, C. L. Hsu, L. J. Li, Y. [illegible], H.Y. Yang, Sci. Rep-uk, 2013, **3**, 1-8.

14 T. Wang , J. Zhuo, K. Du, B. Chen, Z. Zhu, Y. Shao, M. Li, Adv. Mater., 2014, **26**, 3761-3766.

15 Y. Li, H. Wang, L. Xie, Y. Liang, G. Hong, H. Dai, J. Am. Chem. Soc., 2011, **133**, 7296-7299.

16 W. Zhou, K. Zhou, D. Hou, X. Liu, G. Li, Y. Sang, H. Liu, ACS Appl. Mater. Inter., 2014, **6**, 21534-21540.

17 L. Liao, J. Zhu, X. Bian, L. Zhu, M. D. Scanlon, H. H. Girault, [illegible] Liu, Adv. Funct. Mater., 2013, **23**, 5326-5333.

18 S. Chen, J. Duan, Y. Tang, B. Jin, S. Qiao, Nano Energy, 2015, **11**, 11-18.

19 D. Voiry, M. Salehi, R. Silva, T. Fujita, M. Chen, T. Asefa, V. [illegible] Shenoy, G. Eda, and M. Chhowalla, Nano Lett., 2013, **13**, 6222-6227.

20 D. Yang, S. J. Sandoval, W. M. R. Divigalpitiya, J. C. Irwin and [illegible] R. F. Frindt, Phys. Rev. B, 1991, **43**, 12053-12056.

21 J. Bonde, P. G. Moses, T. F. Jaramillo, J. K. Nørskov and I. Chorkendorff, Faraday Discuss., 2008, **140**, 219-231.

22 X. Sun, J. Dai, Y. Guo, C. Wu, F. Hu, J. Zhao, X. Zeng and Y. Xie, Nanoscale, 2014, **6**, 8359-8367.

23 G. Plechinger, S. Heydrich, J. Eroms, D. Weiss, C. Schüller, [illegible] Korn, Appl. Phys. Lett., 2012, **101**, 101906.

24 J. Mann, Q. Ma, P. M. Odenthal, M. Isarraraz, D. Le, Preciado, D. Barroso, K. Yamaguchi, G. V. Palacio, A. Nguyen, T. Tran, M. Wurch, A. Nguyen, V. Klee, S. Bobek, D. Z. Sun, T. [illegible] Heinz, T. S. Rahman, R. Kawakami, L. Bartels, Adv. Mater., 2014, **26**, 1399-1404.

25 H. Li, X. Duan, X. Wu, X. Zhuang, H. Zhou, Q. Zhang, X. Zhu, W. Hu, P. Ren, P. Guo, L. Ma, X. Fan, X. Wang, J. Xu, A. Pan, X. Duan, J. Am. Chem. Soc., 2014, **136**, 3756-3759.

26 R. Dhall, M. R. Neupane, D. Wickramaratne, M. Mecklenburg, Z. Li, C. Moore, R. K. Lake and S. Cronin, Adv. Mater., 2015, **27**, 1573-1578.

27 D. Kong, H. Wang, J. J. Cha, M. Pasta, K. J. Koski, J. Yao, and Y. Cui, Nano Lett., 2013, **13**, 1341-1347.

28 J. Lin, Z. Peng, G. Wang, D. Zakhidov, E. Larios, M. J. Yacaman and J. M. Tour, Adv. Energy Mater., 2014, **4**, 1301875.

29 H. Zhu, M. L. Du, M. Zhang, M. L. Zou, T. T. Yang, Y. Q. Fu and J. M. Yao, J. Mater. Chem. A, 2014, **2**, 7680-7685.

30 K. Chang, D. Geng, X. Li, J. Yang, Y. Tang, M. Cai, R. Li and X. Sun, Adv. Energy Mater., 2013, **3**, 839-844.

31 H. Tang, K. P. Dou, C. C. Kaun, Q. Kuang and S. H. Yang, J. Mater. Chem. A, 2014, **2**, 360-364.

32 Y. Gong, Z. Liu, A. R. Lupini, G. Shi, J. Lin, S. Najmaei, Z. Lin, A. L. Elías, A. Berkdemir, G. You, H. Terrones, M. Terrones, R. Vajtai, S. T. Pantelides, S. J. Pennycook, J. Lou, W. Zhou and P. M. Ajayan, Nano Lett. 2014, 14, 442-449

33 Y. Li, H. Wang, L. Xie, Y. Liang, G. Hong, H. Dai, J. Am. Chem. Soc., 2011, **133**, 7296-7299.